Available online at www.sciencedirect.com
SCIENCE DIRECT
Journal of Molecular Catalysis A: Chemical 246 (2006) 118–127
JOURNAL OF MOLECULAR CATALYSIS A: CHEMICAL
www.elsevier.com/locate/molcata

MCM-41 silica modified with copper and iron oxides as catalysts for methanol decomposition

Tanya Tsoncheva [a,*], Sami Areva [b], Momtchil Dimitrov [a], Daniela Paneva [c], Ivan Mitov [c], Mika Linden [b], Christo Minchev [a]

[a] *Institute of Organic Chemistry, Bulgarian Academy of Sciences, Acad. G. Bonchev bl 9, 1113 Sofia, Bulgaria*
[b] *Department of Physical Chemistry, Abo Akademi University, Porthansgatan 3-5, FI-20500 Turku, Finland*
[c] *Institute of Catalysis, Bulgarian Academy of Sciences, Sofia 1113, Bulgaria*

Received 23 August 2005; received in revised form 19 October 2005; accepted 25 October 2005
Available online 28 November 2005

Abstract

Mixed copper and iron modified MCM-41 mesoporous silica with various Cu/Fe ratio are characterized by N_2 physisorption, X-ray diffraction (XRD), transmission electron micrographs (TEM), X-ray photoelectron spectroscopy (XPS), Moessbauer spectroscopy and temperature programmed reduction with hydrogen. Their catalytic properties in methanol decomposition to CO and H_2 are investigated and compared with that of the corresponding mono-component materials. The catalytic behaviour of bi-component materials are discussed based on the nature of the catalytic active sites.

Keywords: Iron and copper modified MCM-41; Moessbauer spectroscopy; Methanol decomposition

1. Introduction

During the last decade the decomposition of methanol has gained a considerable interest in various aspects such as: obtaining of alternative effective and ecological fuels for vehicles and fuel cells or supplemental fuel for gas turbines at peak demands; preparation of some valuable for the chemical industry compounds, gases or gas mixtures (methyl formate (MF), synthesis gas, methane, etc.); an "energetic pump" for the recovery of heat from the engine exhausts because of its endothermic character and a key for the understanding of mechanism of the reverse methanol synthesis reaction [1–4].

On the other hand, the valuable application of methanol decomposition in various aspects requires the development of catalysts, active at low temperatures in combination with good stability and a high selectivity to the desired product. Copper-based materials have been often studied as good catalysts for methanol decomposition to CO and hydrogen, but the problem with their selectivity at lower temperatures and stability at higher ones still remains [2,5–18]. Much effort for their improvement has been done and various methods such as promoter addition, changes in the copper precursor and preparation conditions have been applied [11–13,15,19,20]. It was shown that the activity and stability of copper-based catalysts is significantly enhanced after their deposition on various porous supports (silica, activated carbon, etc.) [21–25]. However, the decrease of catalysts selectivity due to the formation of methyl formate is observed after their preliminary reduction [21]. In our previous investigation we also found that the process selectivity could be successfully varied to methane formation when iron-based catalysts are used [24,26–32]. Moreover, by variations in the iron phase composition, gas mixtures with different CO/CH_4 ratio could be obtained. It was also assumed, that the iron particles dispersion is of a key importance for the selectivity regulation [26,30]. Larger iron oxide particles, which readily transform to metallic iron or iron carbides due to the influence of the reaction medium, decompose methanol predominantly to CO and H_2. On the contrary, the methane selectivity is essentially increased when transformation of haematite to magnetite occurs.

Several techniques for the catalysts design improvement are known and among them the creation both of nanometer-scale and bimetallic systems have gained substantially popularity recently

* Corresponding author. Tel.: +359 9796640.
E-mail address: tsoncheva@orgchm.bas.bg (T. Tsoncheva).

1381-1169/$ – see front matter © 2005 Elsevier B.V. All rights reserved.
doi:10.1016/j.molcata.2005.10.028

[33,34]. The control and stabilization of nanosized metal/metal oxide species became more available with their deposition on various porous supports [35–42]. Here, the ordered mesoporous silica materials have been widely concerned as new potential carriers for catalysts due to their high specific surface area, pore volume and a narrow pore size distribution [43–52]. The most widely studied mesoporous material is MCM-41, which consists of two-dimensional hexagonal arrays of uniform mesopores with pore diameters ranging from 2 to 10 nm [35,53–59]. MCM-41 is synthesized under alkaline conditions using cationic surfactants as structure directing agents. Furthermore, the use of bimetallic systems is an additional parameter for the catalysts design. The catalytic properties of mixed metal systems could be influenced by the metal/metal oxide particle sizes and it could be quite different when they are in a highly dispersed state due to the altering of their electronic structure [33,60]. The small particle size changes the chemisorption bond strength between the metal surface and the substrate, leading to the appearance of strong metal support interaction (SMSI) with limited reducibility and also leads to the formation of bimetallic nanoparticles. On the other hand, metal/metal oxide dispersion can be readily varied at the addition of second metal due to the formation of mixed oxide phase or oxide interface between the support and the active metal. For the copper–iron-based materials the formation of alloys has been usually established [61,62]. It has been reported that the presence of Fe and Cu in the catalyst significantly influences the sintering and carbidization of iron and/or copper and also improves catalysts activity and stability in reverse water gas shift reaction [63–67]. However, to the best of our knowledge the behaviour of copper–iron catalysts in the process of methanol decomposition has no been reported. The present paper aims at elucidation of the catalytic properties of Cu and Fe supported on MCM-41 materials in methanol decomposition. Special attention is paid on the state of the catalytic active sites.

2. Experimental

2.1. Materials

The parent mesoporous silica of the MCM-41 type with BET surface areas of 1023 m^2/g and total pore volume of 0.85×10^{-6} m^3/g was synthesized by standard procedure [23]. After template removal the parent MCM-41 material was stirred for 1 h first at room temperature and then for 1 h at 323 K with 0.028 M solution of Cu(II) and/or Fe(III) acetylacetonates in chloroform. At the following step the chloroform was evaporated in a rotary evaporator. The sample was then dried at room temperature under vacuum for 3 h. The samples, denoted as *n*CuFe/M41, with total metal content of 6 wt.% and Cu/Fe wt. ratio (*n*) in the range of 0.03–11, were obtained. For comparison, mono-component iron (Fe/M41) and copper (Cu/M41) samples with 6 wt.% metal content, were also prepared.

2.2. Methods of investigation

Small-angle X-ray scattering (SAXS) and powder X-ray diffraction (XRD) measurements were performed on a Kratky compact small-angle system with Cu Kα radiation (wavelength λ = 1.542 Å). The N_2 physisorption was determined at 77 K using a Micromeritics ASAP 2010 sorptometer. The samples were outgassed at 423 K for 12 h before measurements. The pore diameters were determined by NLDFT calculations using Autosorb 1 for Windows 1.25 software (Quantachrome Instruments) [68].

The transmission electron micrographs (TEM) were recorded on Philips CM 30 ST.

The TPR–TGA (temperature-programmed reduction–thermogravimetric analysis) investigations were performed in a Setaram TG92 instrument. Typically, 40 mg of the sample were placed in a microbalance crucible and heated in a flow of 50 vol.% H_2 in Ar (100 cm^3/min) up to 873 K at 5 K/min and a final hold-up of 1 h. Prior to the TPR experiments the samples were treated in situ in a flow of air up to 773 K at a rate of 10 K/min followed by a hold-up of 1 h.

The Moessbauer spectra were obtained at room temperature with a Wissel (Wissenschaftliche Elektronik GmbH, Germany) electromechanical spectrometer working in a constant acceleration mode. A ^{57}Co/Cr (activity ≅ 10 mCi) source and an α-Fe standard were used. The experimentally obtained spectra were fitted by the least square-method. The parameters of hyperfine interaction such as isomer shift (IS), quadruple splitting (QS), the line widths (FWHM), and the relative weight (*G*) of the partial components in the spectra were determined. In order to describe the samples more precisely, an idealized core–shell model is applied to the Moessbauer spectra data [69]. The highest core/shell ratio could be ascribed to the presence of the largest iron particles.

X-ray photoelectron spectroscopy (XPS), measurements (Perkin Elmer PHI 5400 ESCA System Spectrometer) was performed at a base pressure of 1×10^{-8} Torr using the Mg Kα X-ray (λ = 1253.6 eV) source. The electron analyzer pass energy in the XPS high-resolution scans was 35.75 eV. The take-off angle of the photoelectrons was 45°. The UNIFITTU (Version 2.1) software was used for peak fitting and quantitative chemical analysis, applying sensitivity factors given by the manufacturer of the instrument. The high-resolution spectra were charge compensated by setting the binding energy (BE) of the C(1s) contamination peak to 284.6 eV. The atomic surface XPS concentrations were quantitatively estimated using the simplified model of Kerkhof-Moulijn [70].

2.3. Catalytic experiments

The catalytic experiments were carried out in a flow type of reactor (0.055 g of catalyst, three times diluted with grounded glass) with methanol (3.5 mol%) in Ar (50 ml/min), the latter being used as a carrier gas. The temperature was raised with a rate of 1 K/min in the range of 350–770 K. Some experiments were done under isothermal conditions at selected temperatures. On-line gas chromatographic analysis was made on a porapak Q and a molecular sieve column using an absolute calibration method. Before the catalytic experiments the samples were pretreated in situ in air at 773 K for 2 h. In some cases, the samples

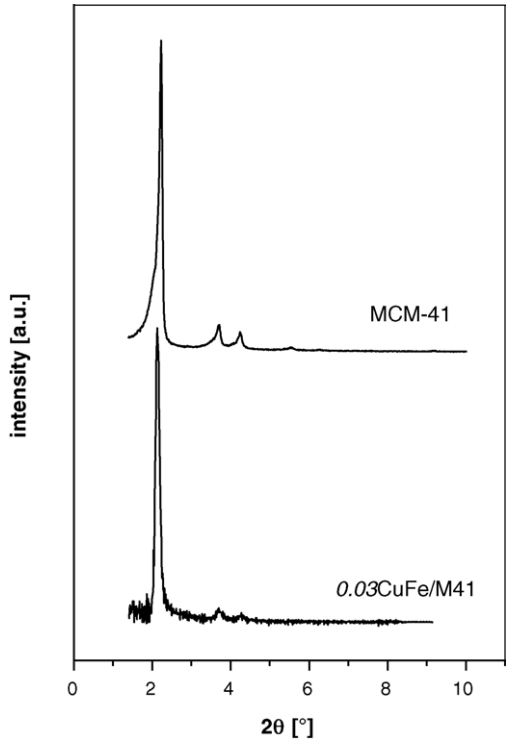

Fig. 1. PXRD for pristine and selected Cu and Fe modified MCM-41 materials.

were additionally reduced with hydrogen at 773 K for 2 h. These samples were denoted as (R).

3. Results

3.1. Textural characterization of the pristine and the Cu and/or Fe modified mesoporous materials

3.1.1. Powder X-ray diffraction and transmission electron microscopy

X-ray diffraction patterns of parent and one example of CuFe-modified silica materials (as the other CuFe loaded materials show similar patterns) are presented in Fig. 1. The preservation of small angles X-ray reflections after the iron and/or copper deposition is an indication for the absence of structural collapse of the silica support during the sample preparation. The observed decrease in the intensity after the impregnation, especially of the high ordered reflections can be ascribed to an overall decrease in the electron density difference between the silica wall and the pore due to the distribution of the iron and copper species within the support pore system.

No additional characteristics of crystalline Fe_2O_3 (24.1°, 33.0°, and 35.6° 2θ) and CuO (35.7° and 38.5° 2θ) were observed in the P-XRD pattern (not shown), indicative of the presence of highly dispersed iron and copper oxide particles. An additional evidence for their high dispersion are the TEM images of the samples (Fig. 2).

Table 1
Samples composition and results of N_2 physisorption measurement

Sample	Cu/Fe	BET (m^2/g)	d_{pore} (BJH) (nm)	V_{pore} (BJH) (m^3/g)
MCM-41		1023	2.98	1.15
Fe/M41		902	2.98	0.96
Cu/M41		845	2.98	0.91
0.03CuFe/M41	0.03	928	2.98	1.02
2CuFe/M41	2	879	2.98	0.94
8CuFe/M41	8	901	2.97	1.03
11CuFe/M41	11	855	2.96	0.92

3.1.2. Nitrogen physisorption

Nitrogen adsorption/desorption curves and the corresponding calculated characteristics of the parent silica and its iron and/or copper oxide modifications are presented in Fig. 3a and Table 1, respectively. In Fig. 3b the changes in the support pore diameter distribution due to the metals introduction, calculated by Barret–Joyner–Halenda (BJH) theory [71] are also shown. These BJH pore diameters do not give the absolute pore diameters, because the theory is not corrected for materials with pore diameters below 4 nm, but they give reasonable result for comparison. The isotherms of the parent MCM-41 material is of type IV profile according to IUPAC classification, which is typical of

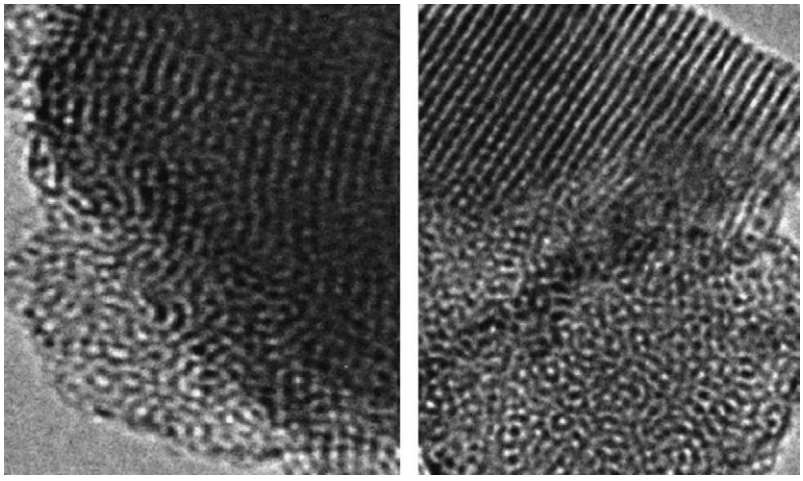

Fig. 2. TEM images of 0.03CuFe/M41 and 2CuFe/M41 initial samples.

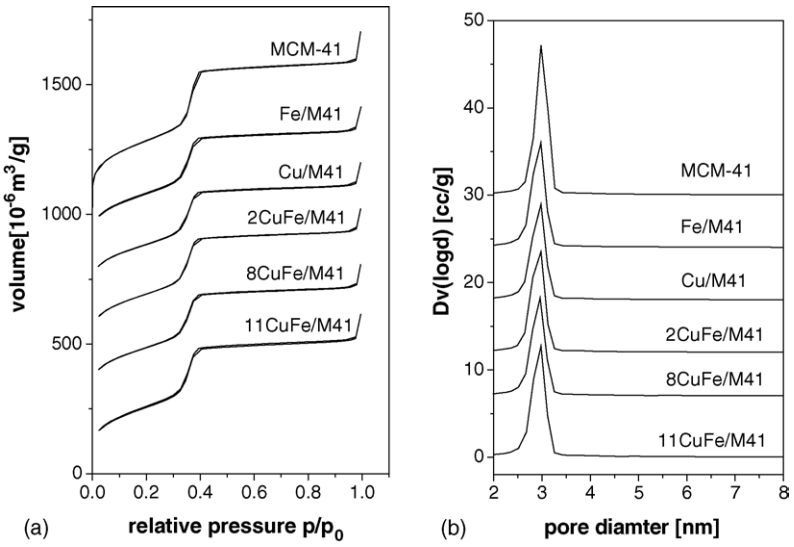

Fig. 3. N_2 physisorption isotherms (a) and corresponding pore diameter distribution (b) for pristine and Fe and/or Cu modified MCM-41 materials.

mesoporous materials. A sharp pores filling step at 0.3–0.4 relative pressure was observed, which indicates a narrow pore size distribution. Similar nitrogen sorption isotherms with a somewhat less pronounced condensation step were obtained for all modified samples (Fig. 3a). Generally, the sorption isotherms and X-ray diffraction measurements indicate that the mesoscopic order is maintained after the impregnation and the latter did not alter or harm the general pore characteristics of the silica support.

3.2. Spectral measurements

3.2.1. Moessbauer spectroscopy

In order to characterize the state of iron for the obtained materials more precisely, Moessbauer spectra of the initial mono-component Fe/M41 and selected bi-component *n*CuFe/M41 samples with different Cu/Fe ratio were obtained. The Moessbauer spectra are presented in Fig. 4a and the corresponding calculated parameters are listed in Table 2. The spectra of all materials consist of lines of quadrupole doublets (Dbl) due to small particle effects. The determined IS values (Dbl1 and Dbl2, Table 2) are characteristic for high spin Fe(III) ions in octahedral coordination. They could be assigned to highly dispersed iron oxide particles with superparamagnetic behaviour (SPM). In accordance with the calculated core/shell ratios (Table 2), almost similar iron particles dispersion despite the samples composition could be assumed in all cases.

Moessbauer spectra (Fig. 4b and c) and the corresponding parameters (Table 2) for the samples after Sections 3.3 and 3.4 were also presented. For the mono-component Fe/M41, the main changes concern the appearance of a new component (Dbl3) of Fe(II) clusters. Their relative weight is greater after the TPR experiment as compared to that after the catalytic test. Surprisingly, such type of transformations was not observed for any

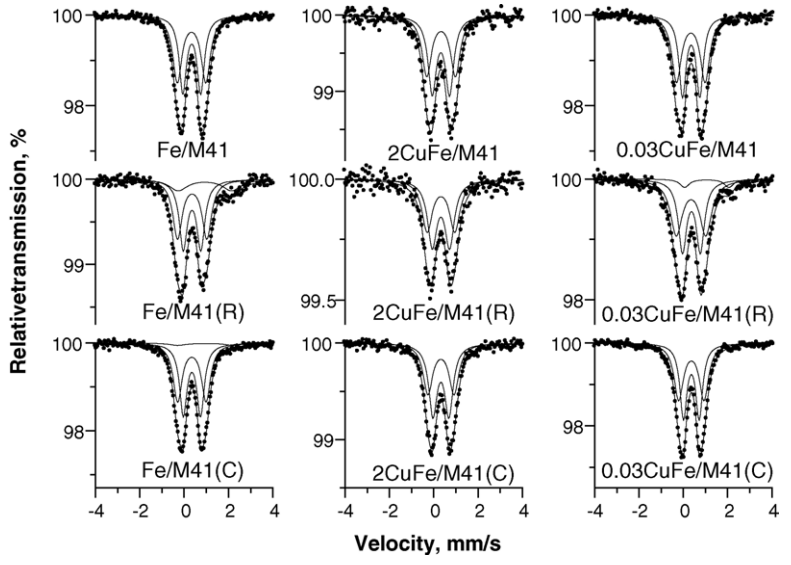

Fig. 4. Moessbauer spectra of air pretreated, reduced (R) and treated in the catalysis (C) Fe/M41, 2CuFe/M41 and 0.03CuFe/M41 materials.

Table 2
Moessbauer parameters of the selected samples after air pretreatment (O), reduction (R) and catalytic test (C)

Sample	Compounds	IS (mm/s)	QS (mm/s)	FWHM (mm/s)	*G* (%)
Fe/M41	Dbl 1–Fe_2O_3–SPM–core	0.33	0.81	0.39	48
	Dbl 2–Fe_2O_3–SPM–shell	0.34	1.29	0.50	52
Fe/M41 (R)	Dbl 1–Fe_2O_3–SPM–core	0.36	0.79	0.43	42
	Dbl 2–Fe_2O_3–SPM–shell	0.36	1.32	0.51	42
	Dbl 3–Fe (II) cluster	0.94	2.41	1.00	16
Fe/M41(C)	Dbl 1–Fe_2O_3–SPM–core	0.35	0.78	0.40	48
	Dbl 2–Fe_2O_3–SPM–shell	0.35	1.28	0.49	48
	Dbl 3–Fe(II) cluster	0.97	2.52	1.00	4
2CuFe/M41	Dbl 1–Fe_2O_3–SPM–core	0.33	0.78	0.45	52
	Dbl 2–Fe_2O_3–SPM–shell	0.33	1.29	0.52	48
2CuFe/M41(R)	Dbl 1–Fe_2O_3–SPM–core	0.33	0.78	0.51	53
	Dbl 2–Fe_2O_3–SPM–shell	0.33	1.25	0.57	47
2CuFe/M41(C)	Dbl 1–Fe_2O_3–SPM–core	0.33	0.72	0.45	55
	Dbl 2–Fe_2O_3–SPM–shell	0.33	1.18	0.52	45
0.03CuFe/M41	Dbl 1–Fe_2O_3–SPM–core	0.36	0.71	0.38	49
	Dbl 2–Fe_2O_3–SPM–shell	0.36	1.14	0.50	51
0.03CuFe/M41(R)	Dbl 1–Fe_2O_3–SPM–core	0.36	0.81	0.44	44
	Dbl 2–Fe_2O_3–SPM–shell	0.35	1.33	0.64	50
	Dbl 3–Fe(II) cluster	1.06	2.00	0.50	6
0.03CuFe/M41(C)	Dbl 1–Fe_2O_3–SPM–core	0.35	0.78	0.38	47
	Dbl 2–Fe_2O_3–SPM–shell	0.34	1.29	0.52	53

of bi-component materials after the catalytic test. Only in the case of the sample with lowest copper content (0.03CuFe/M41), Fe(II) species but in very low relative weight, were observed after hydrogen reduction.

3.2.2. XPS measurements

Data from XPS measurements for the mono-component Cu and Fe MCM-41 supported materials and selected bi-component ones with different Cu/Fe ratio are presented in Fig. 5. The atomic percentage ratios of various species are listed in Table 3. Two distinct iron peaks were observed at binding energies of 711.4 and 714.5 eV for the Fe/M41 sample. The binding energy of about 711 eV for the Fe 2p3/2 main peak is in agreement with the typical values for the iron oxides reported in the literature [72–74]. The peak at higher BE could not be attributed to any one particular iron state. Thus, when combining the observed slightly higher BE value for the Fe(III) specie compared to the literature values and the small Fe/Si ratio it can be concluded that the two peaks originate from the core level of the deposited iron particle and from its surface atoms associated with the support, resulting in the reduction in their coordination number. Similarly, the iron peaks for *n*CuFe/M41 samples can be concluded to result from Fe(III) species with the core level atoms and the surface atoms interacting differently with the support, although their corresponding binding energies were slightly lower than for the Fe/M41 sample i.e. 710.1 and 713.1 eV, respectively. The observed lower BE values for the bi-component materials as compared to the expected that ones of hematite could be also ascribed to the decrease of the Fe–O bond strength due to the existence of additional type of metal species interaction [75]. All bi-component samples contain only one type of Cu atoms, namely Cu(II).

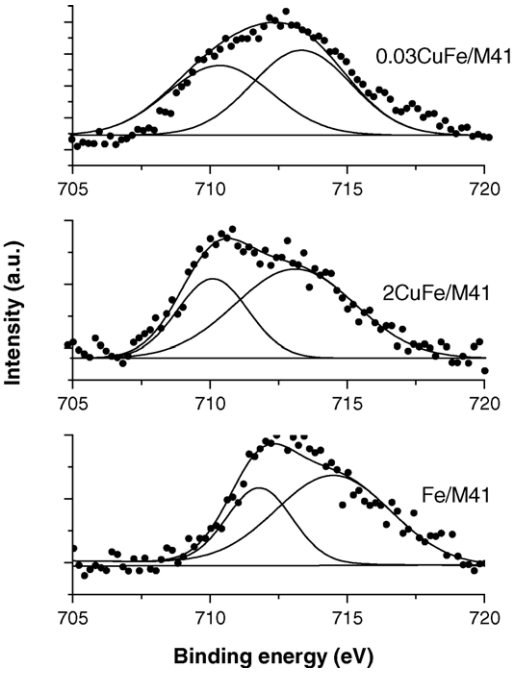

Fig. 5. XPS spectra of the selected samples.

Table 3
Surface atomic concentration of various species for the selected samples elucidated by XPS

Sample	Fe/Si	Cu/Si	Fe/Cu
0.03CuFe/M41	0.045	0.004	11.25
2CuFe/M41	0.032	0.017	1.88
Cu/M41	–	0.024	–
Fe/M41	0.029	–	–

Table 4
Data of TPR experiments for Fe and/or Cu modified MCM-41

Sample	T_{max}[a] (K)	Weight loss (mg)		Reduction degree[b] (%)	LT/HT ratio
		LT stage	HT stage		
0.03CuFe/M41	574	0.22	0.27	62.8	0.81
2CuFe/M41	453	0.23	0.35	95.1	0.65
8CuFe/M41	444	0.18	0.23	100	0.78
11CuFe/M41	452	0.40	0.25	100	1.6
Cu/M41	442	0.26	0.42	100	0.62
Fe/M41	572	0.24	0.43	76	0.56

[a] Temperature of the low-temperature reduction maximum in the DTG curves.
[b] Total weight loss during the low-temperature (LT) and high-temperature (HT) stages referenced to the calculated theoretical weight loss for the reduction of the corresponding metal ion to pure metal.

3.3. TPR experiments

The data from TPR–TG experiments of all iron and/or copper modified materials are presented in Table 4 and Fig. 6. From the TG profiles (not shown) could be distinguished the presence of two reduction stages, a low-temperature (LT) and a high-temperature (HT) one that could be ascribed to the reduction of metal oxide species with different dispersion. For all copper containing materials the LT stage is characterized by a clearly defined reduction peak with maximum at about 440–460 K corresponding to Cu(II) → Cu(0) transition. Only in the case of 0.03CuFe/M41 a clearly defined reduction peak with maximum at about 575 K is registered that we assign to Fe(III) → Fe(II) transitions. Similar reductive behaviour is observed for Fe/M41 as well. At higher temperatures only a tail in the TG profile is observed, which could be assigned to the presence of iron and/or copper oxide species reducible with greater difficulty due to their higher dispersion and stronger interaction with the support. For Fe/M41 and 0.03CuFe/M41 a comparatively low reduction degree, probably due to presence of significant amount of reducible with greater difficulty iron oxide species is observed. For more precise elucidation of the different reductive behaviour of the samples we have calculated the LT/HT weight loss ratio (Table 4). The observed increase in the LT/HT ratio for all bi-component materials in comparison with the corresponding mono-component ones suggests a decrease in the relative part of the particles strongly interacting with the support.

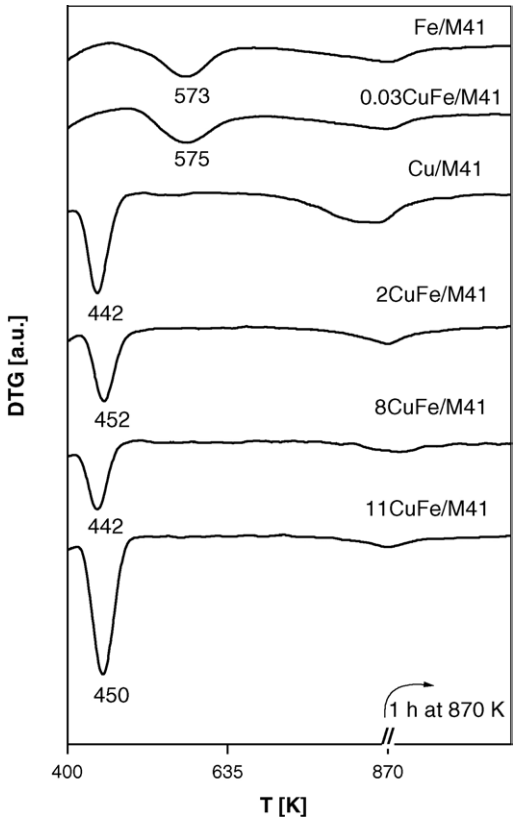

Fig. 6. DTG curves registered during TPR of various Cu and/or Fe modified MCM-41.

3.4. Catalytic results

In Fig. 7 are presented the temperature dependencies of methanol decomposition and CO selectivity for the samples with

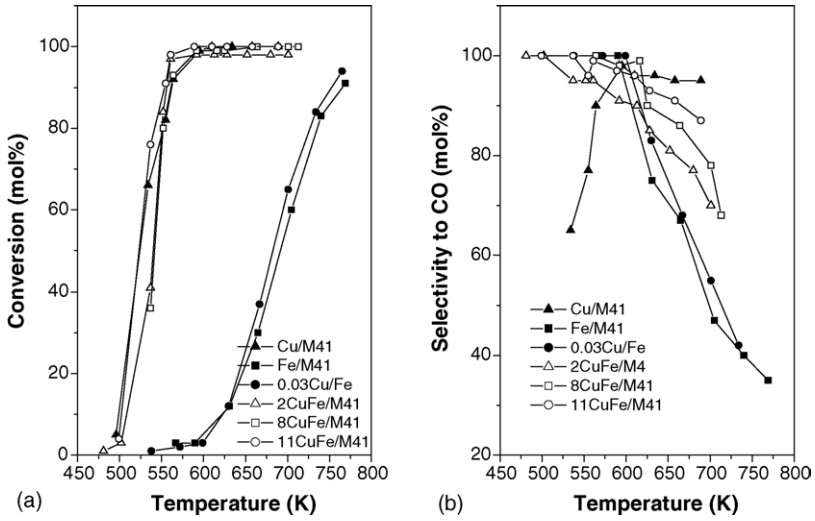

Fig. 7. Methanol conversion (a) and CO selectivity (b) vs. temperature for the investigated various copper and iron modified MCM-41 silicas.

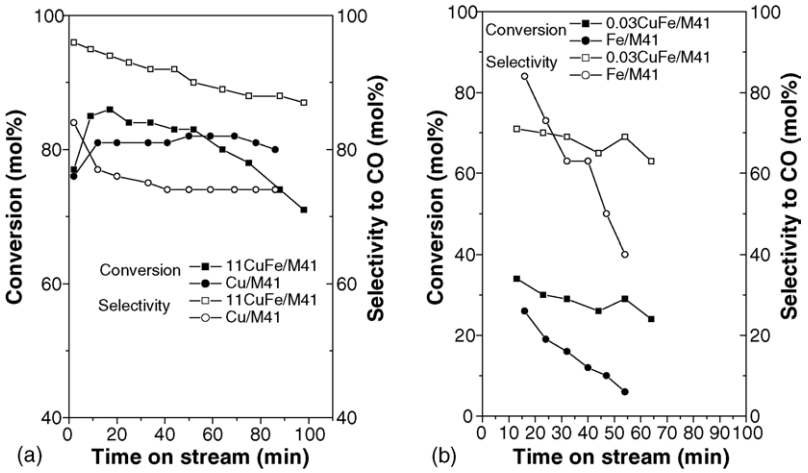

Fig. 8. Methanol conversion and CO selectivity vs. time on stream at 562 K for 11CuFe/M41 (a) and at 650 K for 0.03CuFe/M41 (b), compared with Cu/M41 at the same temperatures.

various Cu/Fe ratios. For comparison, the catalytic properties of the corresponding mono-component materials are also shown. As a whole, bi-component materials exhibit similar catalytic activity to that of Cu/M41 with well-defined conversion loop at 500–550 K. Only the sample with the lowest copper content (0.03CuFe/M41), which exhibit a bit higher catalytic activity in comparison with Fe/M41, shows a shift of the conversion curve at significantly higher temperatures. At the same time similarly to Fe/M41, almost 100% selectivity to CO is registered at relatively lower temperatures for all copper–iron materials (Fig. 7b). Under the same conditions a significant formation of methyl formate (MF) is registered for Cu/M41. However, above 600 K changes in the CO selectivity for all the samples occur. A decrease in CO selectivity due to the formation of methane is found for all iron containing materials and that ability is more pronounced for the samples with higher iron content. At the same time, a well-defined tendency for CO selectivity increase with temperature is observed for Cu/M41.

The increase in the CO selectivity for the selected *n*CuFe/M41 samples with highest (11CuFe/M41) and lowest (0.03CuFe/M41) copper content under isothermal conditions is demonstrated in Fig. 8a and b, respectively. A well-defined tendency for the conversion and catalytic stability increase are observed for 0.03CuFe/M41, while they essentially decrease for 11CuFe/M41.

In Fig. 9 is illustrated the effect of the preliminary reduction of the selected *n*CuFe/M41 sample and it is compared with that one of the corresponding mono-component materials. A decrease in both methanol conversion and methane selectivity occurs after the reduction of Cu/M41 and Fe/M41. However, no significant catalytic effect of the pretreatment conditions is found for 2CuFe/M41. For comparison, a mechanical mixture of Cu/M41 and Fe/M41 (2:1) is also studied after pretreatment in air and hydrogen (Fig. 10). In contrast to the corresponding 2CuFe/M41 (Fig. 7) here a complex conversion curve characterized with lower catalytic activity and a maximum at about

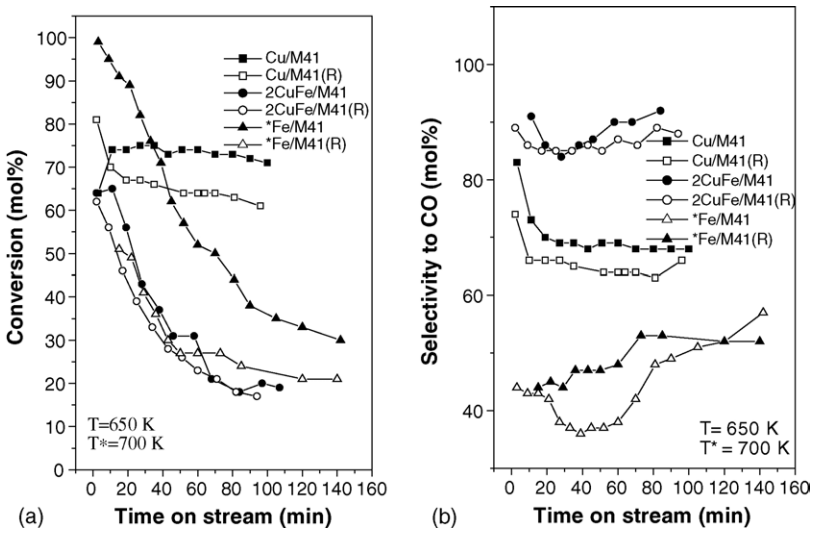

Fig. 9. Methanol conversion (a) and CO selectivity (b) vs. time on stream for selected materials pretreated in air or hydrogen (R).

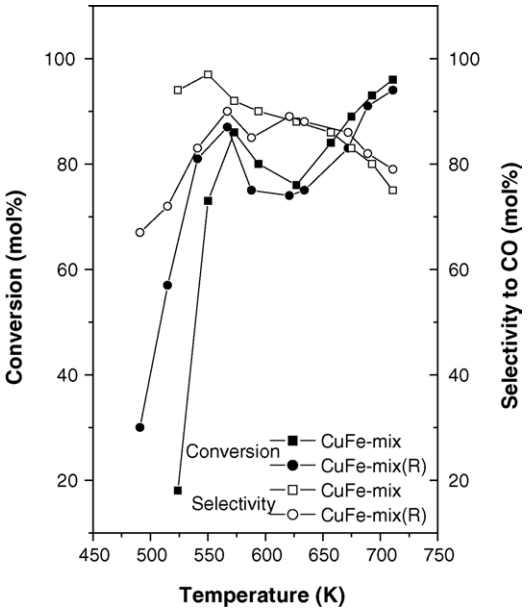

Fig. 10. Methanol conversion for mechanical mixture of Cu/M41 and Fe/M41 (2:1) pretreated in air or hydrogen (R).

580 K is registered. Some differences in the CO selectivity of the mixed sample depending on the pretreatment medium are also observed.

4. Discussion

The methanol decomposition selectivity has been widely discussed in the literature. Various possible reaction pathways leading to the formation of CO, hydrogen, methane, methyl formate, etc. have been suggested [9,17,76–79]. For the copper containing catalysts, methyl formate is often assumed to be the first product formed in methanol decomposition to CO and H_2, while over group VIII metals, methanol could be directly converted to CO and hydrogen. The mechanisms included the formation of HCHO as an intermediate was proposed in both cases. However, HCHO adsorption preferentially as η^1(O) structure is suggested for the copper containing catalysts. This structure favours its attack by nucleophiles (such as CH_3OH, CH_3O) leading to the formation of MF. It is suggested also that for group VIII metals, HCHO intermediates exist as η^2(C,O) structures which can be readily decomposed to CO and H_2. An alternative pathway including methane formation through the preferential C–O bond cleavage in the methanol molecule has been also discussed [78,79].

Based on the presented results above, some general catalytic effects should be mentioned:

(i) In a wide range of Cu/Fe ratio, the samples preserve similar, but substantially more unstable catalytic activity in comparison with the mono-component Cu-containing material (Figs. 7 and 8). However, practically no methyl formate is registered at relatively low temperatures, but a significant decrease in CO selectivity due to the formation of methane is observed at higher temperatures.

(ii) Addition of very small amounts of Cu- to iron-based materials (0.03CuFe/M41) leads not only to substantial increase and stabilization of the catalytic activity (Fig. 8a), but also to a decrease in the methane selectivity (Fig. 8b).

(iii) The preliminary reduction of the samples with hydrogen essentially affects the catalytic behaviour only for the mono-component materials, while no significant effect is observed for the bi-component ones (Fig. 9).

(iv) The catalytic behaviour of the mechanical mixture of Cu/M41 and Fe/M41 differs essentially from that one of *n*CuFe/M41 material with the corresponding Cu/Fe ratio (Figs. 7 and 10).

The data from the N_2 physisorption, XRD, TEM, XPS and Moessbauer spectra (see Section 3) show the formation of Cu(II) and/or Fe(III) finely dispersed oxide particles into the silica matrix. The simultaneous appearance in TPR profiles of low temperature and high temperature reduction stages, usually characterized with LT/HT weight loss ratio below one, is indication for the presence of reducible with greater difficulty particles, probably strongly interacting with the support (Table 4). The same conclusion could be also assumed on the base of XPS spectra, where two well-defined iron peaks with different BE, probably belonging to iron species differently interacting with the support are registered (Table 3, Fig. 5) However, some essential differences in the state of metal species for the *n*CuFe/M41 samples as compared to the mono-component materials are observed:

(i) Moessbauer spectra for the bi-component materials show that no or very small transformations with iron particles occur during the reduction or after the catalytic test. On the contrary, Fe(II) clusters in various relative weights are found for the mono-component Fe/M41 sample after the catalysis or reduction treatment (Table 2, Fig. 4).

(ii) The surface atomic Fe/Cu ratio elucidated in XPS measurements remains above one, despite the samples composition. Here, some shifting of the BE values for the iron species in comparison with the mono-component Fe/M41 sample is also registered (Table 3).

(iii) An increase in the LT/HT weight loss ratio in TPR profiles for all *n*CuFe/M41 in comparison with the corresponding mono-component materials is observed (Table 4).

So, some substantial changes in the state of copper and iron particles during their simultaneous introduction in the samples is assumed. The formation of new, complex catalytic active center of Cu–Fe_x type, which is not a “mechanical mixture” of individual copper and iron sites, could be suggested. This is in agreement with [63], where new active species located at the interface between Cu and Fe was also proposed. In this aspect, changes in the electron donation between the catalytic site and the substrate (methanol) molecule leading to the changes in the adsorption properties could occur. As a result, changes in the catalytic activity, stability and selectivity due to the variations in the methanol decomposition mechanism are expected.

5. Conclusion

At lower temperatures copper–iron modified MCM-41 mesoporous silica exhibit both higher catalytic activity and CO selectivity in comparison with the corresponding mono-component materials. The catalytic behaviour of the samples is gradually influenced by the Cu/Fe ratio. The formation of complex catalytic active centre, including Fe(III) and Cu(II) species in various ratio is assumed.

Acknowledgements

Financial supports by the Bulgarian National Scientific Fund (X-1208) and by the Bulgarian-Finland interacademic exchange is acknowledged. Ch. M. also wishes to thank to the Deutscher Akademischer Austauschdienst. Ch. M. and T.T. thank to Prof. Dr. M. Fröba for TEM measurements.

References

[1] J. Agrell, B. Lindström, L.J. Pettersson, S. Jaras, Catalysis 16 (2002) 67.
[2] W.H. Cheng, Acc. Chem. Res. 32 (1999) 685.
[3] M.P. Kapoor, Y. Matsumura, J. Mol. Catal. A: Chem. 178 (2002) 169.
[4] J.S. Lee, J.C. Kim, Y.G. Kim, Appl. Catal. 57 (1990) 1.
[5] J. Zawadzki, B. Azambre, O. Heintz, A. Krzton, J. Weber, Carbon 38 (2000) 509.
[6] W.H. Cheng, Mater. Chem. Phys. 41 (1995) 36.
[7] W.H. Cheng, Appl. Catal. A 130 (1995) 13.
[8] W.H. Cheng, C.Y. Shiau, T.H. Liu, H.L. Tung, J.F. Lu, C.C. Hsu, Appl. Catal. 170 (1998) 15.
[9] N.W. Cant, S.P. Tonner, D.L. Trimm, M.S. Wainwright, J. Catal. 91 (1985) 197.
[10] S. Sato, M. Iijima, T. Nakayama, T. Sodesawa, F. Nozaki, J. Catal. 169 (1997) 47.
[11] K. Hashimoto, N. Toukai, J. Mol. Catal. A: Chem. 186 (2002) 79.
[12] M. Clement, Y. Zhang, D.S. Brands, E.K. Poels, A. Bliek, Stud. Surf. Sci. Catal. 130 (2000) 2123.
[13] I.A. Fisher, A.T. Bell, J. Catal. 184 (1999) 357.
[14] D.B. Clarke, D.K. Lee, M.J. Sandoval, A.T. Bell, J. Catal. 150 (1994) 81.
[15] L. Domokos, T. Katona, A. Molnar, Catal. Lett. 40 (1996) 215.
[16] M. Ai, Appl. Catal. 11 (1984) 259.
[17] K. Takagi, Y. Moricawa, T. Ikawa, Chem. Lett. (1985) 527.
[18] T.P. Minyukova, I.I. Simentsova, A.V. Khasin, N.V. Shtertser, N.A. Baronskaya, A.A. Khassn, T.M. Yurieva, Appl. Catal. A 237 (2002) 171.
[19] T. Sodesawa, M. Nagacho, A. Onodera, F. Nozaki, J. Catal. 102 (1986) 460.
[20] A. Guerro-Ruiz, I. Rodriguez Ramos, J.L.G. Fierro, Appl. Catal. 72 (1991) 119.
[21] T. Tsoncheva, Tz. Venkov, M. Dimitrov, C. Minchev, K. Hadjiivanov, J. Mol. Catal. A: Chem. 209 (2003) 125.
[22] R. Nickolov, T. Tsoncheva, D. Mehandjiev, Fuel 81 (2002) 203.
[23] C. Minchev, R. Köhn, T. Tsoncheva, M. Dimitrov, M. Fröba, Stud. Surf. Sci. Catal. 135 (2001) 253.
[24] C. Minchev, R. Koehn, T. Tsoncheva, M. Dimitrov, I. Mitov, D. Paneva, H. Huwe, M. Froeba, Stud. Surf. Sci. Catal. 142B (2002) 1245.
[25] T. Tsoncheva, S. Vankova, D. Mehandjiev, Fuel 82 (2003) 755.
[26] R. Köhn, D. Paneva, M. Dimitrov, T. Tsoncheva, I. Mitov, C. Minchev, M. Fröba, Microporous Mesoporous Mater. 63 (2003) 125.
[27] C. Minchev, H. Huwe, T. Tsoncheva, M. Dimitrov, D. Paneva, I. Mitov, M. Froeba, in: E. van Steen et al. (Eds.), Proceedings of the 14th Int. Zeol. Conf., South Africa, 2004, p. 841.
[28] T. Tsoncheva, D. Paneva, I. Mitov, H. Huwe, M. Fröba, M. Dimitrov, C. Minchev, React. Kinet. Catal. Lett. 83 (2004) 299.
[29] C. Minchev, H. Huwe, T. Tsoncheva, D. Paneva, M. Dimitrov, I. Mitov, M. Fröba, Microporous Mesoporous Mater. 81 (2005) 333.
[30] T. Tsoncheva, M. Dimitrov, D. Paneva, I. Mitov, R. Köhn, M. Fröba, C. Minchev, React. Kinet. Catal. Lett. 74 (2001) 385.
[31] D. Paneva, T. Tsoncheva, E. Manova, I. Mitov, T. Ruskov, Appl. Catal. A: Gen. 267 (2004) 67.
[32] E. Manova, T. Tsoncheva, D. Paneva, I. Mitov, K. Tenchev, L. Petrov, Appl.Catal. A: Gen. 277 (2004) 119.
[33] L. Guczi, Catal. Today 101 (2005) 53.
[34] H.H. Kung, M.C. Kung, Catal. Today 87 (2004) 219.
[35] F. Schüth, A. Wingen, J. Sauer, Microporous Mesoporous Mater. 44–45 (2001) 465.
[36] A. Taguchi, F. Schüth, Microporous Mesoporous Mater. 77 (2005) 1.
[37] F. Martinez, Y.-J. Han, G. Stucky, J.L. Sotelo, G. Ovejero, J.A. Metero, Stud. Surf. Sci. Catal. 142 (2002) 1109.
[38] Z.Y. Yuan, W. Zhou, Z.L. Zhang, Q. Chen, B.L. Su, L.M. Peng, Stud. Surf. Sci. Catal. 141 (2002) 403.
[39] M. Fröba, R. Köhn, G. Bouffaund, O. Richard, G. Van Tendeloo, Chem. Mater. 11 (1999) 2858.
[40] T. Abe, Y. Tachibana, T. Uematsu, M. Iwamoto, J. Chem. Soc., Chem. Commun. (1995) 1617.
[41] M. Iwamoto, T. Abe, Y. Tachibana, J. Mol. catal. A 155 (2000) 143.
[42] W.-H. Zhang, J.-L. Shi, L.-Z. Wang, D.-S. Yan, Chem. Mater. 12 (2000) 1408.
[43] J.Y. Ying, C.P. Mehnert, M.S. Wong, Angew. Chem. Int. Ed. 38 (1999) 56.
[44] F. Schüth, Chem. Mater. 13 (2001) 3184.
[45] W. Schmidt, F. Schüth, Adv. Mater. 14 (2002) 629.
[46] A. Stein, Adv. Mater. 15 (2003) 763.
[47] D. Zhao, Q. Huo, J. Feng, B.F. Chmelka, G.D. Stucky, J. Am. Chem. Soc. 120 (1998) 6024.
[48] Y. Sakamoto, M. Kaneda, O. Terasaki, D.Y. Zhao, J.M. Kim, G.D. Stucky, H.J. Shin, R. Ryoo, Nature 408 (2000) 449.
[49] J. Fan, C.Z. Yu, T. Gao, J. Lei, B.Z. Tian, L.M. Wang, Q. Luo, B. Tu, W.Z. Zhou, D.Y. Zhao, Angew. Chem. Int. Ed. 42 (2003) 3146.
[50] G. Zheng, H. Zhu, Q. Luo, Y. Zhou, D. Zhao, Chem. Mater. 13 (2001) 2240.
[51] T. Yamada, H.S. Zhou, H. Uchida, M. Tomita, Y. Ueno, T. Ichano, I. Honma, K. Asai, T. Katsube, Adv. Mater. 14 (2002) 812.
[52] S. Besson, T. Gacoin, C. Rricolleau, C. Jecquiod, J.-P. Boilot, Nano Lett. 2 (2002) 409.
[53] A. Davidson, Curr. Opin. Colloid Interface Sci. 7 (2002) 92.
[54] A. Corma, Chem. Rev. 97 (1997) 2373.
[55] U. Ciesla, F. Schüth, Microporous Mesoporous Mater. 27 (1999) 131.
[56] R. Köhn, M. Fröba, Catal. Today 68 (2001) 227.
[57] S.E. Dapurkar, S.K. Badamali, P. Selvam, Catal. Today 68 (2001) 63.
[58] C.T. Kresge, M.E. Leonowicz, W.J. Roth, J.C. Vartuli, Nature 359 (1992) 170.
[59] J.S. Beck, J.C. Vartuli, W.J. Roth, M.E. Leonowicz, C.T. Kresge, K.D. Schmitt, C.T.-W. Chu, D.H. Olson, E.W. Sheppard, S.B. McCullen, J.B. Higgings, J.L. Schlenker, JACS 114 (1992) 10834.
[60] A.Yu. Stakheev, L.M. Kustov, Appl. Catal. A: Gen. 188 (1999) 3.
[61] R. Vollmer, S.V. Dijken, M. Schleberger, J. Kirschner, Phys. Rev. B 61 (2000) 1303.
[62] S.S.A. Razee, R. Prasad, R.M. Singru, J. Phys. B 9 (1997) 4455.
[63] C.-S. Chen, W.-H. Cheng, S.-S. Lin, Appl. Catal. A: Gen. 257 (2004) 97.
[64] S. Li, G.D. Meitzner, E. Iglesia, J. Phys. Chem. B 105 (2001) 5743.
[65] M.A. Edwards, D.M. Whittle, C. Rhodes, A.M. Ward, D. Rohan, M.D. Shannon, G.J. Hutchings, C.J. Kiely, Phys. Chem. Chem. Phys. 4 (2002) 3902.
[66] S. Li, S. Krishnamoorthy, A. Li, G.D. Meitzer, E. Iglesia, J. Catal. 206 (2002) 202.
[67] M.E. Dry, in: J.R. Anderson, M. Boudart (Eds.), Catalysis Science and Technology, vol. 1, Springer-Verlag, New York, 1981, p. 159.

[68] A. Lind, C. von Hohenesche, J.-H. Smått, M. Linden, K.K. Unger, Microporous Mesoporous Mater. 66 (2003) 219.
[69] M. Van der Kraan, Hyperfine Interact. 40 (1988) 211.
[70] V. Leon, Surf. Sci. 339 (1995) 931.
[71] E.P. Barret, L.G. Joyner, P.P. Halenda, JACS 73 (1951) 373.
[72] Y. Yuan, W. Cao, W. Weng, J. Catal. 228 (2004) 311–320.
[73] C.-T. Wang, S.-H. Ro, Appl. Catal. A: Gen. 285 (2005) 196–204.
[74] A.P. Grosvenor, B.A. Kobe, N.S. Tougaard, W.N. Lennard, Surf. Interface Anal. 36 (2004) 1564.
[75] T. Fujii, F.M.F. deGroot, G.A. Sawatzki, F.C. Voogt, T. Hibma, K. Okada, Phys. Rev. B 59 (1999) 3195.
[76] N. Takezawa, N. Iwasa, Catal. Today 36 (1997) 45.
[77] M. Mavrikakis, M.A. Barteau, J. Mol. Catal. A: Chem. 131 (1998) 135.
[78] R.J. Levis, J. Zhicheng, N. Winograd, J. Am. Chem. Soc. 110 (1988) 4431.
[79] R.J. Levis, J. Zhicheng, N. Winograd, J. Am. Chem. Soc. 111 (1989) 4605.